A function for tyrosine phosphorylation of type 1 inositol 1,4,5-trisphosphate receptor in lymphocyte activation

Nikhil deSouza,[1] Jie Cui,[1] Miroslav Dura,[1] Thomas V. McDonald,[2,3] and Andrew R. Marks[1]

[1]Department of Physiology and Cellular Biophysics, Clyde and Helen Wu Center for Molecular Cardiology, Columbia University College of Physicians and Surgeons, New York, NY 10032
[2]Department of Medicine and [3]Department of Molecular Pharmacology, Albert Einstein College of Medicine, New York, NY 10461

Sustained elevation of intracellular calcium by Ca^{2+} release–activated Ca^{2+} channels is required for lymphocyte activation. Sustained Ca^{2+} entry requires endoplasmic reticulum (ER) Ca^{2+} depletion and prolonged activation of inositol 1,4,5-trisphosphate receptor (IP_3R)/Ca^{2+} release channels. However, a major isoform in lymphocyte ER, IP3R1, is inhibited by elevated levels of cytosolic Ca^{2+}, and the mechanism that enables the prolonged activation of IP_3R1 required for lymphocyte activation is unclear. We show that IP_3R1 binds to the scaffolding protein linker of activated T cells and colocalizes with the T cell receptor during activation, resulting in persistent phosphorylation of IP_3R1 at Tyr353. This phosphorylation increases the sensitivity of the channel to activation by IP_3 and renders the channel less sensitive to Ca^{2+}-induced inactivation. Expression of a mutant IP3R1-Y353F channel in lymphocytes causes defective Ca^{2+} signaling and decreased nuclear factor of activated T cells activation. Thus, tyrosine phosphorylation of IP3R1-Y353 may have an important function in maintaining elevated cytosolic Ca^{2+} levels during lymphocyte activation.

Introduction

T cell activation is initiated by the engagement of the antigen/major histocompatibility complex with the T cell receptor (TCR), triggering the formation of the immunological synapse (Yokosuka et al., 2005). The immunological synapse is a dynamic, highly ordered structure that includes adaptor proteins and kinases, including the nonreceptor Src tyrosine kinases Lck and Fyn (Monks et al., 1998; Bromley et al., 2001). Once activated, these kinases trigger a phosphorylation cascade that leads to the activation of PLCγ-1, which hydrolyzes phosphotidylinositol 4,5 bisphosphate into diacylglycerol and inositol 1,4,5-trisphosphate (IP_3; Koretzky and Myung, 2001). IP_3 triggers Ca^{2+} release from the ER by activating the IP_3 receptor (IP_3R; Berridge and Irvine, 1984). ER Ca^{2+} depletion is sensed by stromal interaction molecule 1 (STIM1), an EF hand containing ER transmembrane protein (Liou et al., 2005; Roos et al., 2005). ER Ca^{2+} depletion triggers the redistribution of STIM1 such that STIM1 forms more discrete puncta at junctional ER sites near the plasma membrane (Zhang et al., 2005; Luik et al., 2006; Wu et al., 2006). STIM1 communicates the loss of ER Ca^{2+} to the plasma membrane Ca^{2+} release–activated Ca^{2+} (CRAC) channels (Feske et al., 2006; Vig et al., 2006), which colocalize with STIM1 (Luik et al., 2006; Wu et al., 2006). Activation of CRAC channels triggers sustained Ca^{2+} influx, which is referred to as capacitative Ca^{2+} entry (Putney et al., 2001). Additionally, plasma membrane–localized IP_3Rs potentially contribute to Ca^{2+} influx upon T lymphocyte activation (Dellis et al., 2006). Sustained elevation of intracellular Ca^{2+} ($[Ca^{2+}]_i$) causes nuclear factor of activated T cells (NFAT) nuclear translocation, eventually leading to interleukin-2 (IL-2) production (Shibasaki et al., 1996; Lewis, 2001).

During T cell activation, $[Ca^{2+}]_i$ elevation persists for hours after the initial activation event (Huppa et al., 2003), and sustained $[Ca^{2+}]_i$ elevation requires prolonged IP_3R-mediated Ca^{2+} release to keep the ER Ca^{2+} depleted, ensuring sustained Ca^{2+} influx. However, upon lymphocyte activation, global $[IP_3]$ is only transiently increased and rapidly decreases within 10 min after stimulation (Guse et al., 1993; Sei et al., 1995). Moreover, IP_3R1 channel activity is inhibited by increasing $[Ca^{2+}]_i$ (>300 nM Ca^{2+}; Bezprozvanny et al., 1991) and the channel would be

Correspondence to A.R. Marks: arm42@columbia.edu

Abbreviations used in this paper: BCR, B cell receptor; $[Ca^{2+}]_i$, intracellular Ca^{2+}; CRAC, Ca^{2+} release–activated Ca^{2+}; HEK, human embryonic kidney; IL-2, interleukin-2; IP_3, inositol 1,4,5-trisphosphate; IP_3R, IP_3 receptor; LAT, linker of activated T cells; NFAT, nuclear factor of activated T cells; PM, plasma membrane; STIM1, stromal interaction molecule 1; TCR, T cell receptor; TK, thymidine kinase; WT, wild type.

The online version of this article contains supplemental material.

The Journal of Cell Biology, Vol. 179, No. 5, December 3, 2007 923–934
http://www.jcb.org/cgi/doi/10.1083/jcb.200708200

closed when exposed to the cytosolic [Ca^{2+}] achieved during lymphocyte activation (Lewis, 2001). Thus, there must be a mechanism that enables IP_3R channels to remain open when exposed to cellular conditions of globally decreasing [IP_3] and elevated [$Ca^{2+}]_i$.

In neurons, which require elevated [IP_3] (10–15 μM) to trigger IP_3R activation and rapid ER Ca^{2+} release (Khodakhah and Ogden, 1993; Svoboda and Mainen, 1999), PLC-coupled receptors cocluster with IP_3Rs, forming "signaling microdomains" to ensure efficient IP_3R activation by creating locally elevated [IP_3] (Delmas et al., 2002; Delmas and Brown, 2002). Similarly, in activated T cells, IP_3R1 cocaps with the TCR at sites of T cell activation (Khan et al., 1992), where the cellular IP_3-generating machinery, specifically linker of activated T cells (LAT) and PLCγ-1, also accumulate (Douglass and Vale, 2005; Espagnolle et al., 2007).

We had previously demonstrated that upon T cell activation, IP_3R1 is phosphorylated by the Src family kinase Fyn. Additionally, in planar lipid bilayer studies, we observed that tyrosine-phosphorylated IP_3R1 exhibits a higher open probability at ∼700 nM [Ca^{2+}] than nonphosphorylated IP_3R1 (Jayaraman et al., 1996). Thus, IP_3R tyrosine phosphorylation could provide a mechanism that would allow sustained channel activation even as cytosolic [Ca^{2+}] is in the range of 500–1,000 nM (Lewis, 2001), thereby maintaining a depleted ER Ca^{2+} store.

We identified IP_3R1-Y353, located in the IP_3-binding domain, as a key tyrosine phosphorylation site on IP_3R1 that is phosphorylated during lymphocyte activation (Cui et al., 2004). We generated IP_3R-deficient lymphocyte cell lines expressing a recombinant IP_3R1 mutant (IP_3R1-Y353F) that cannot be tyrosine phosphorylated at this key regulatory site. This allowed us to assess the effect of IP_3R1 tyrosine phosphorylation on Ca^{2+} dynamics upon lymphocyte activation.

We show that in activated Jurkat T cells, Y353-phosphorylated (phosphoY353) IP_3R1 clusters and colocalizes with the TCR. In cell spreading assays, the clustered Y353-phosphorylated IP_3R1 forms a distinct ER substructure, facilitating the formation of a TCR-Y35–phosphorylated IP_3R1 signaling microdomain. Y353-phosphorylated IP_3R1 staining was clearly detectable for at least 1 h after T cell activation, suggesting that tyrosine phosphorylation of the channel is prolonged. In single channel studies, Y353-phosphorylated IP_3R1 increased IP_3R1 channel activity at physiological [IP_3] and decreased Ca^{2+}-dependent channel inactivation. IP_3R-deficient B cells stably expressing IP_3R1-Y353F exhibited decreased ER Ca^{2+} release, oscillations, and influx in response to B cell receptor (BCR) activation. Additionally, Jurkat T cells expressing IP_3R1-Y353F exhibited a blunted NFAT response upon T cell activation, suggesting that phosphorylation of IP_3R1 at Y353 is important for robust T cell activation.

Results

IP_3R1 phosphoY353 colocalizes with the TCR upon T cell activation

Previous studies showed that the TCR cocaps with IP_3R1 upon T cell activation (Khan et al., 1992). We wanted to examine if phosphorylation at Y353 altered the ability of IP_3R1 to cocap with the TCR upon T cell activation. Using an IP_3R1-Y353 phosphoepitope-specific antibody, we observed uniformly distributed weak basal Y353 phosphorylation in unstimulated cells with the distribution resembling that of IP_3R1 on the ER. In unstimulated T cells, the TCR/CD3 fluorescence was uniformly distributed on the plasma membrane (Fig. 1 A, top). However, upon T cell activation, both TCR/CD3 and IP_3R1 phosphoY353 showed a dramatic colocalization to one site in the cell, forming a tight cluster at the site of stimulation (Fig. 1 A). Additionally, the intensity of the immunofluorescence signal for IP_3R1 phosphoY353 increased significantly upon T cell activation. Preincubation of the phosphoY353 antibody with a blocking peptide decreased the phosphoY353 signal in activated T cells, confirming that the phosphoepitope antibody was specific for IP_3R1 phosphoY353 (Fig. 1 A, bottom).

Additionally, we wanted to determine if the cocapping event observed upon T cell activation triggered association of IP_3R1 with upstream regulators of the IP_3-generating enzyme PLCγ-1. Coimmunoprecipitation assays identified LAT as a protein that associated with IP_3R1 upon T cell activation (Fig. 1 B). LAT is tyrosine phosphorylated by ZAP-70 in activated T cells and the phosphorylation of LAT is essential for ensuring the robust activation of PLCγ-1 (Sommers et al., 2002). In ZAP-70–deficient T cells, LAT did not coimmunoprecipitate with IP_3R1 (Fig. 1 B), which suggests that the association of IP_3R1 with LAT is mediated by phosphorylation of LAT by ZAP-70.

The activation-dependent cocapping of IP_3R1 phosphoY353 with the TCR and the association of IP_3R1 with LAT, an essential component of the IP_3-generating machinery, suggest that a signaling microdomain forms upon T cell activation whereby IP_3R1 is found in close proximity to the IP_3-generating machinery.

IP_3R1 phosphoY353 forms a spatially restricted ER substructure colocalized with the TCR

Because IP_3R1 is primarily expressed on the ER, we wanted to determine whether IP_3R1 phosphoY353 clustering represented a general ER reorganization or a specific reorganization of IP_3R1 phosphoY353. We performed CD3-stimulated cell spreading assays by staining stimulated Jurkat T cells with the luminal ER membrane protein calnexin. Upon T cell activation, calnexin staining remained uniformly distributed throughout the cell, indicating that in Jurkat T cells, the ER does not generally reorganize upon ER Ca^{2+} release (Fig. 2 A), which is consistent with previously published findings (Luik et al., 2006; Wu et al., 2006). In contrast, the TCR staining showed a strong central focal point with less intense punctate staining extending out to the periphery of the cell (Fig. 2 A). Global phosphotyrosine staining colocalized with the TCR staining is also shown (Fig. 2 A, top). The bottom of Fig. 2 A shows a 3D reconstruction image of the surface immunofluorescence detected in the examined cell slice. Consistent with the 2D images, the calnexin ER staining appears to be uniformly distributed, in contrast to the centrally localized TCR signal, which suggests that no gross changes to the ER occur upon activation. In stimulated cells, IP_3R1 phosphoY353 colocalized with both the TCR and phosphotyrosine staining (Fig. 2 B).

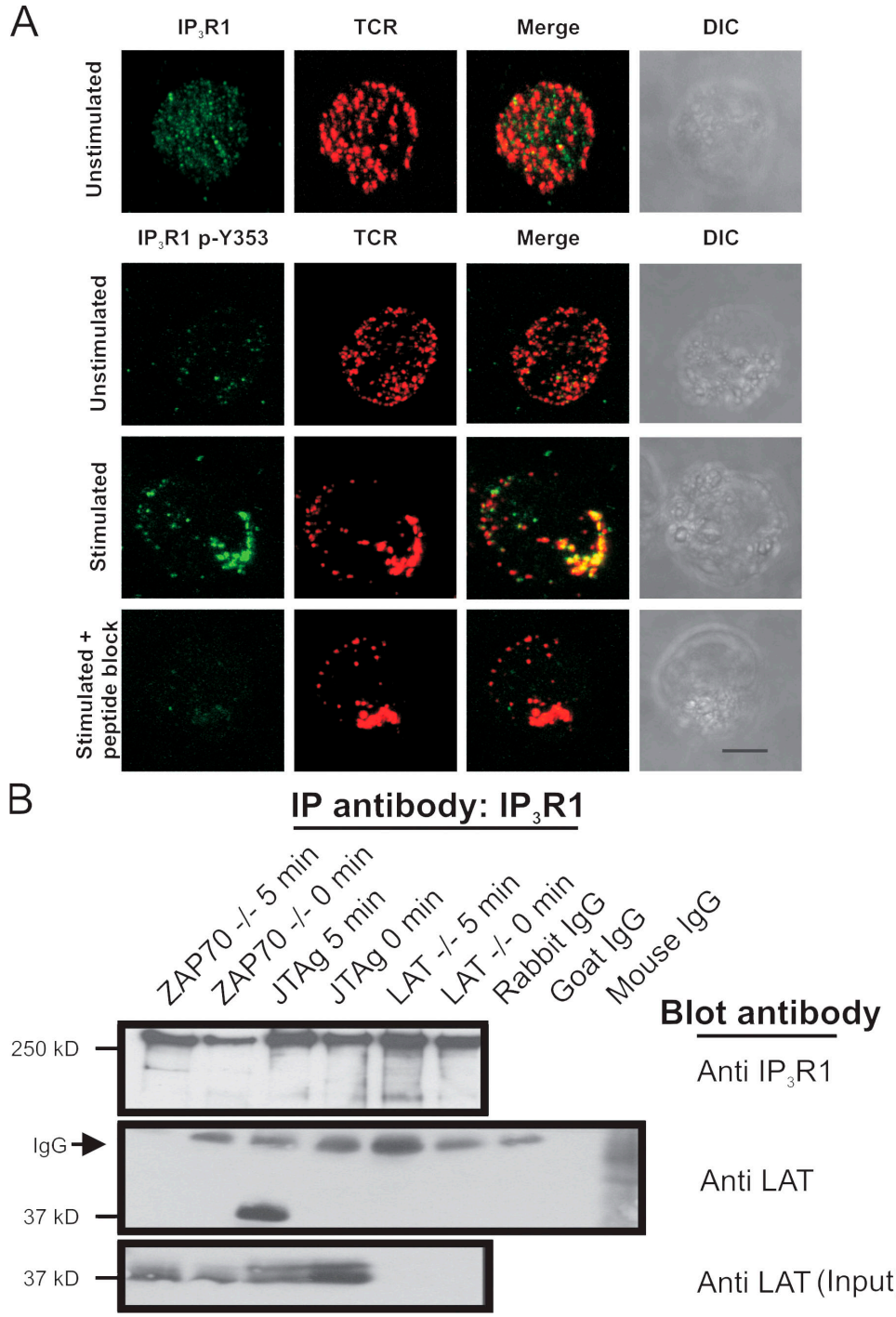

Figure 1. **Colocalization of IP_3R1 phosphoY353 with TCR upon stimulation.** (A) Jurkat T cells were incubated with mouse mAb against CD3 (OKT3) and a TRITC-conjugated goat anti–mouse antibody. Cells were fixed and stained with either an antibody against IP_3R1 or a phosphoepitope-specific antibody against IP_3R1 phosphoY353. Cells were examined using confocal microscopy and projection images are shown. Unstimulated T cells were examined for IP_3R1 and TCR/CD3 localization. (top) IP_3R1 localization is shown in green and TCR/CD3 localization is shown in red. The far right shows differential interference contrast images. Unstimulated T cells were examined for IP_3R1 phosphoY353 and TCR/CD3 localization. (second from the top) IP_3R1 phosphoY353 localization is shown in green and TCR/CD3 localization is shown in red. (third from the top) The localization of IP_3R1 phosphoY353 and TCR/CD3 in T cells stimulated for 5 min. (bottom) Peptide block–mediated quenching of the IP_3R1 phosphoY353 signal in T cells stimulated for 5 min. Approximately 30% of cells responded by displaying a reorganized, well-formed cap structure. Of that population, a majority of cells showed a robust increase in Y353 phosphorylation signal and colocalization of Y353 with the TCR. Bar, 5 μm. (B) Coimmunoprecipitation of IP_3R1 with LAT in activated Jurkat T cells. Lysate from 2×10^8 cells was incubated with anti-IP_3R1 antibody to immunoprecipitate IP_3R1 and blotted with anti-IP_3R1 (top). (middle) Coimmunoprecipitation of LAT with IP_3R1 with association occurring only in activated Jurkat T cells and not in LAT-deficient cells (LAT−/−) used as negative control or ZAP70 null cells (ZAP70−/−), suggesting a phosphorylation-mediated association between LAT and IP_3R1. The arrow designates the IgG signal from the immunoprecipitating antibody. (bottom) The endogenous LAT levels in the various T cell lines used.

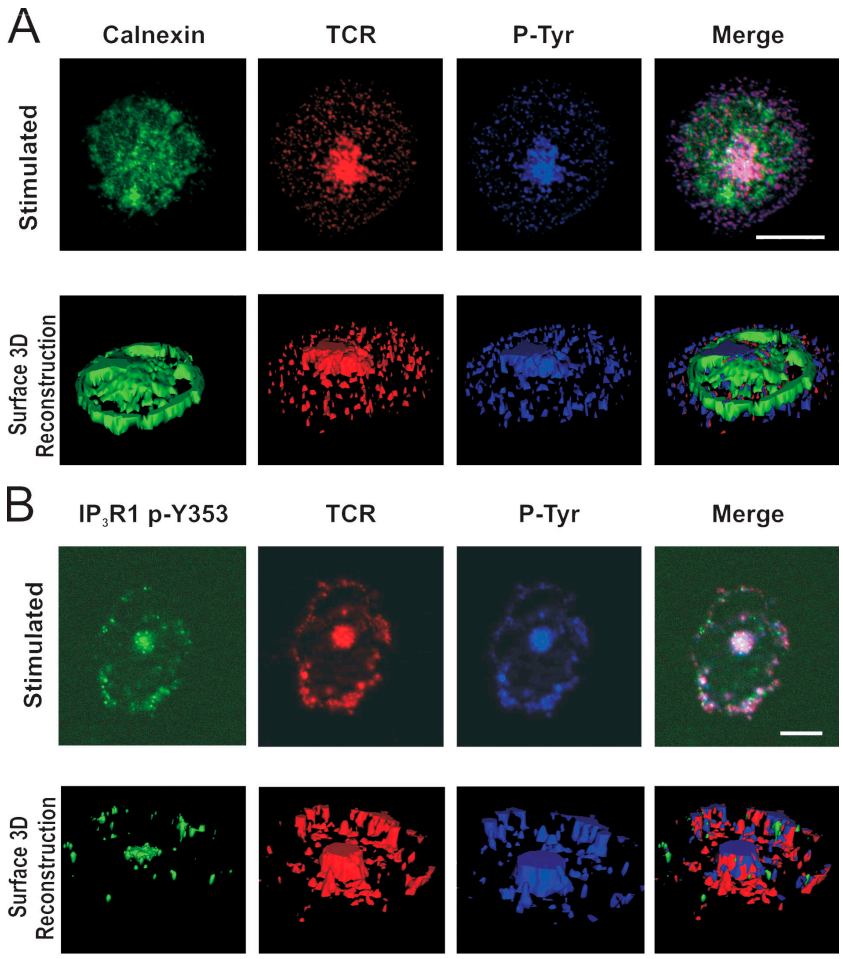

Figure 2. **IP_3R1 phosphoY353 forms a spatially restricted signaling microdomain with TCR.** (A, top) Calnexin staining of ER in stimulated T cells in cell spreading assay. Jurkat T cells were incubated on CD3-coated coverslips for 5 min and stained for calnexin (green), TCR/CD3 (red), and total phosphotyrosine (blue). (bottom) 3D rendering of image slice shown on top. The 3D rendering reveals global distribution of ER upon T cell activation. In the cell spreading assay, ~70% of cells appeared to be stimulated (formed a central TCR cluster). Of that population, almost all the cells showed colocalization of Y353 with the TCR. (B, top) Staining of IP_3R1 phosphoY353 in stimulated T cells. Jurkat T cells were incubated on CD3-coated coverslips for 5 min and stained for IP_3R1 phosphoY353 (green), TCR/CD3 (red), and total phosphotyrosine (blue). (bottom) 3D rendering of image slice shown on top. The 3D rendering reveals localization of IP_3R1 phosphoY353 to a discrete site colocalizing with TCR and phosphotyrosine with localization potentially mediated by the extrusion of the ER membrane. Bars, 5 μm.

3D reconstruction of the surface fluorescence showed that IP_3R1 phosphoY353 largely colocalized with the TCR signal, in sharp contrast to the calnexin staining (Fig. 2 B, bottom).

Collectively, these data suggest that upon T cell stimulation, IP_3R1 phosphoY353 undergoes a lateral redistribution along the ER membrane, accumulating in spatially restricted domains where it colocalizes with the TCR.

Persistent IP_3R1 Y353 phosphorylation is detectable after T cell activation

We had previously determined that Y353 was robustly tyrosine-phosphorylated by 3 min after T cell stimulation (Cui et al., 2004). To further explore the dynamics of Y353 tyrosine phosphorylation upon T cell activation, we stimulated Jurkat T cells by incubating the cells on anti-CD3 antibody–coated coverslips. IP_3R1-Y353 phosphorylation was strongest between 2 and 5 min after T cell activation, in agreement with our previously published data (Cui et al., 2004). Y353 phosphorylation was still detectable at 60 min after the initial T cell activation event (Fig. 3, A and B).

IP_3R1-Y353 phosphorylation increases receptor sensitivity to IP_3

To determine if the increased affinity of tyrosine-phosphorylated IP_3R1 for IP_3 (Cui et al., 2004) alters IP_3-mediated IP_3R1 channel open probability, we conducted single-channel measurements using microsomes generated from human embryonic kidney (HEK) cells transiently cotransfected with either wild-type (WT) IP_3R1 and constitutively active Fyn (Fyn Y528F) representing WT-IP_3R1 phosphorylated at Y353, WT-IP_3R1 and a kinase-dead mutant Fyn (Fyn K296M) representing unphosphorylated WT-IP_3R1, or IP_3R1-Y353F and Fyn Y528F representing WT-IP_3R1, which cannot be phosphorylated at Y353. At [IP_3] ranging from 100 nM to 5 μM, tyrosine-phosphorylated IP_3R1 exhibited higher open probabilities compared with the mutant IP_3R1-Y353F, with an ~4.5-fold decrease in K_d (WT-IP_3R1, 0.710 μM ± 0.05, vs. IP_3R1-Y353F, 3.264 μM ± 0.05; Fig. 4 A), which is consistent with the increased IP_3 sensitivity of Y353-phosphorylated WT-IP_3R1. WT-IP_3R1 coexpressed with a kinase-dead Fyn mutant exhibited channel activity comparable to IP_3R1-Y353F channels (Fig. 4 B). Specifically, the channel activity of phosphorylated WT-IP_3R1 was higher than that of IP_3R1-Y353F or unphosphorylated IP_3R1 at 2 μM IP_3 and 173 nM Ca^{2+} (Fig. 4 B). Indeed, phosphorylated WT-IP_3R1 exhibited an approximately threefold increase in channel open probability in comparison to both IP_3R1-Y353F and unphosphorylated IP_3R1 (Fig. 4 B), suggesting that Fyn phosphorylation of IP_3R1 at Y353 increases channel activity and that Y353 is a key regulatory Fyn phosphorylation site on IP_3R1.

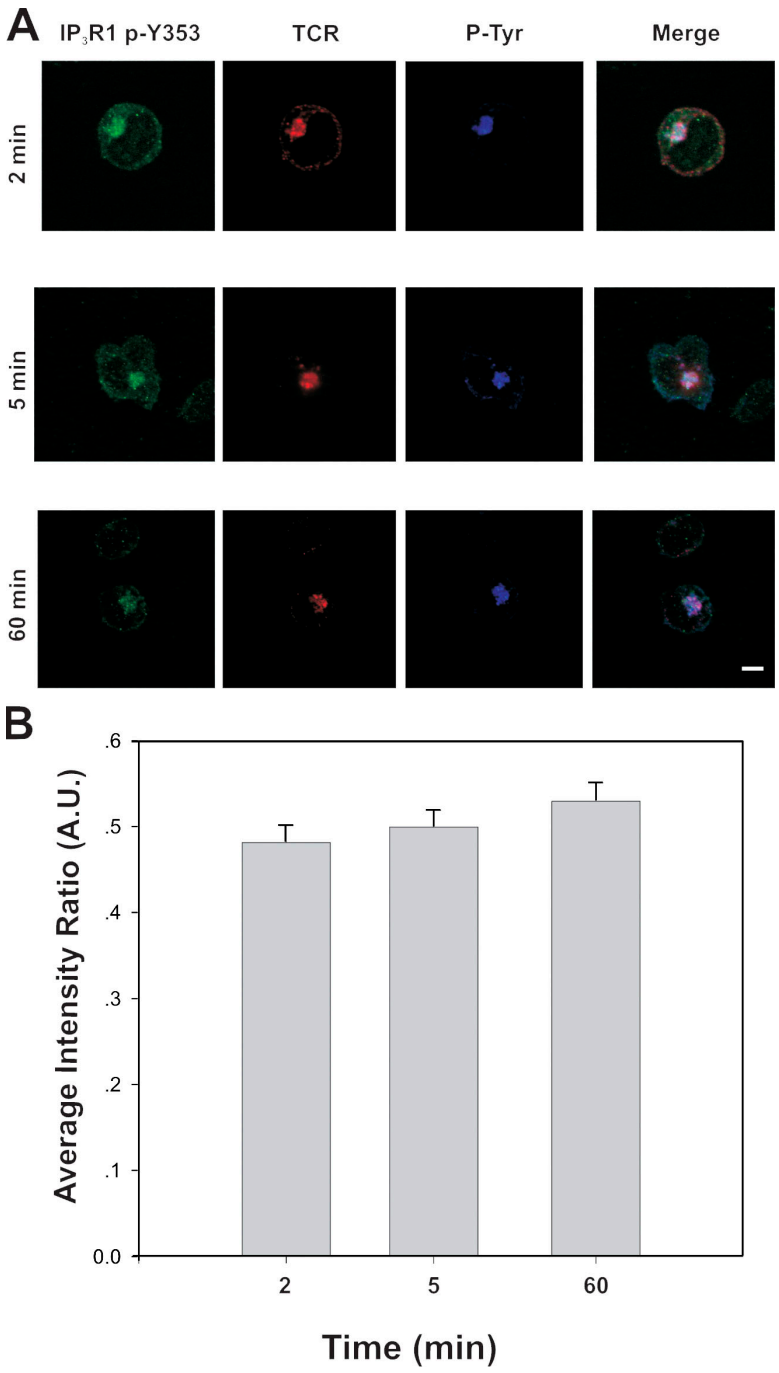

Figure 3. **Persistent IP_3R1-Y353 phosphorylation detectable after T cell activation.** (A) Examining the duration of IP_3R1-Y353 phosphorylation upon T cell activation in a cell spreading assay. Immunofluorescence staining of phosphorylated IP_3R1-Y353 was examined at 2, 5, and 60 min. IP_3R1-Y353 phosphorylation was detectable even 60 min after the initial activation event. Bar, 5 μm. (B) Quantification of clustering of phosphorylated IP_3R1-Y353 in relation to overall TCR clustering in activated T cells. The percentage of activated T cells also displaying clustering of IP_3R1 phosphoY353 was determined at various time points including 2, 5, and 60 min. Fluorescence was still observed 60 min after the initial T cell activation event. Approximately 50 cells were examined for each group from three separate experiments. Error bars represent the SEM.

Collectively, these data suggest that IP_3R1-Y353 phosphorylation helps maintain IP_3R1 in the open state, even as $[IP_3]$ levels decline after activation.

IP_3R1-Y353 phosphorylation reduces Ca^{2+}-dependent IP_3R1 channel inactivation

Having demonstrated that tyrosine phosphorylation of IP_3R1 results in increased channel open probability over a range of $[IP_3]$, we now wanted to determine whether tyrosine phosphorylation modulates the sensitivity of IP_3R1 to Ca^{2+}-dependent channel inactivation. IP_3R1 channel activity exhibits a bell-shaped dependence on cytosolic $[Ca^{2+}]$, being activated at low $[Ca^{2+}]$ (~200–300 nM) and inactivated at higher $[Ca^{2+}]$ (Bezprozvanny et al., 1991; Yoneshima et al., 1997; Kaznacheyeva et al., 1998; Picard et al., 1998). In addition to being activated by IP_3, IP_3R1 has to remain open at elevated cytosolic $[Ca^{2+}]$ to allow Ca^{2+}-dependent lymphocyte activation to proceed.

To determine whether phosphorylation of IP_3R1-Y353 can modulate the Ca^{2+}-dependent regulation of the channel, we examined the single channel properties of the channel in response to a physiological range of $[Ca^{2+}]$ in the presence of 2 μM IP_3. At $[Ca^{2+}]$ that has been shown to inhibit unphosphorylated WT-IP_3R1 (>200–300 nM; Bezprozvanny et al., 1991), tyrosine-phosphorylated WT-IP_3R1 exhibited a significantly higher open

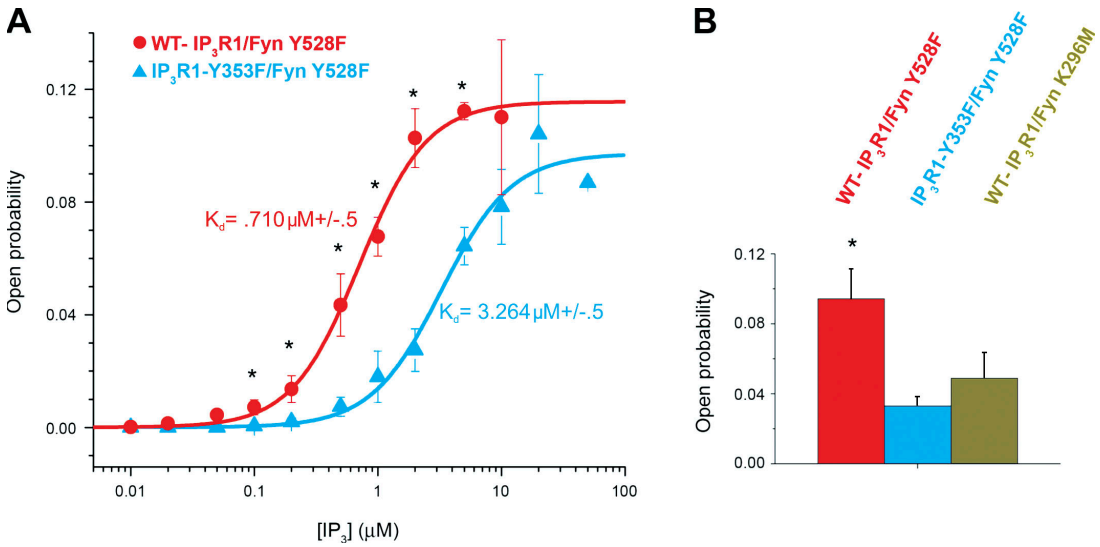

Figure 4. **Tyrosine phosphorylation of IP_3R1 increases the receptor's IP_3 sensitivity.** (A) IP_3 sensitivity of the channel in the planar lipid bilayer. Channel activity of Fyn-phosphorylated IP_3R1 (WT-IP_3R1/Fyn Y528F) and phosphorylated IP_3R1-Y353F (IP_3R1-Y353F/Fyn Y528F) was measured at 173 nM of free cytosolic Ca^{2+} in the presence of 2 μM ruthenium red, 1 mM Na-ATP, and various IP_3 concentrations (10 nM to 10 μM). Open probability values at each IP_3 concentration were calculated as a mean from several independent experiments ($n = 4$ for WT-IP_3R1/Fyn Y528F; $n = 7$ for IP_3R1-Y353F/Fyn Y528F; *, $P < 0.05$ WT vs. Y353F by *t* test) and fitted by the equation described by Tang et al. (2003). (B) Comparison of open probability for Fyn-phosphorylated WT-IP_3R1, Fyn-phosphorylated IP_3R1-Y353F, and WT-IP_3R1 coexpressed with kinase-dead Fyn (unphosphorylated WT-IP_3R1). At 173 nM Ca^{2+} and 2 μM IP_3, Fyn-phosphorylated WT-IP_3R1 exhibits an approximately threefold increase in channel open probability as compared with both IP_3R1-Y353F and unphosphorylated WT-IP_3R1 (*, $P < 0.05$ phosphorylated WT vs. Y353F and phosphorylated vs. unphosphorylated WT by *t* test). Error bars represent the SEM.

probability (threefold increase, $P < 0.05$, $n > 3$ for each channel type) than IP_3R1-Y353F (Fig. 5 A). Mean open times and current amplitudes were similar for both WT-IP_3R1 and IP_3R1-Y353F (Fig. 5 B). To determine whether the increased open probability of the tyrosine-phosphorylated WT-IP_3R1 was influenced by its increased sensitivity to [IP_3] compared with IP_3R1-Y353F, we also compared the activity of these channels at 10 and 100 μM [IP_3]. At both 10 and 100 μM IP_3, the difference in channel activity between tyrosine-phosphorylated WT-IP_3R1 and IP_3R1-Y353F was not significant (unpublished data). Thus, tyrosine phosphorylation of Y353 on IP_3R1 increases channel open probability and reduces Ca^{2+}-dependent channel inactivation at [Ca^{2+}] of ~200–1,000 nM, which is comparable to the level of sustained $[Ca^{2+}]_i$ observed upon lymphocyte activation.

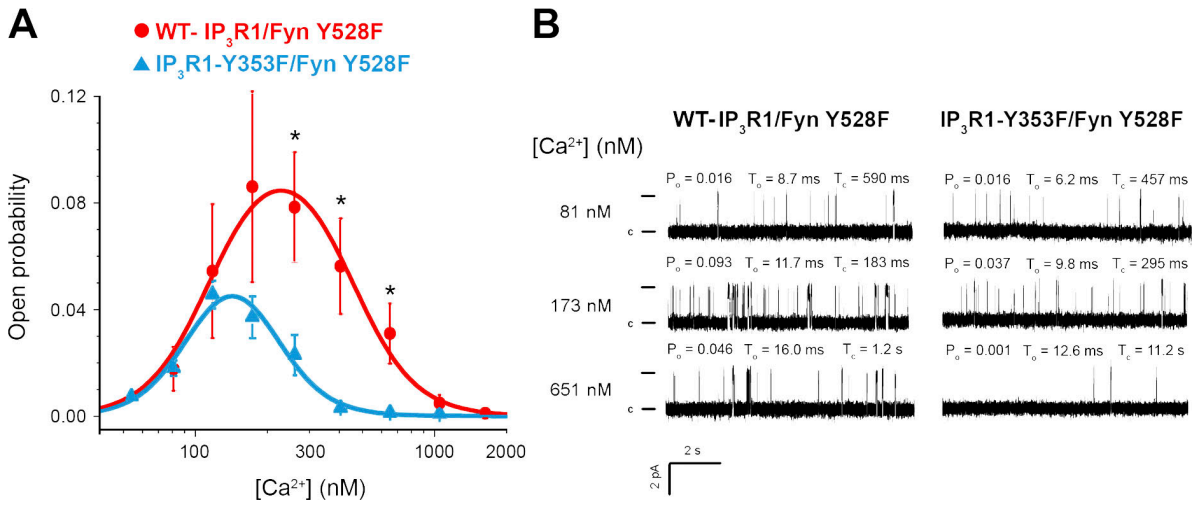

Figure 5. **Ca^{2+} dependence of WT-IP_3R1 and IP_3R1-Y353F single-channel activity.** (A) A comparison of the open probability of Fyn-phosphorylated WT-IP_3R1 and phosphorylated IP_3R1-Y353F at varying Ca^{2+} concentrations. The activity of the channel was measured in the presence of 2 μm IP_3, 2 μM ruthenium red, and 1 mM Na-ATP at different Ca^{2+} concentrations ranging from 50 nM to 2.5 μM. Each data point represents the open probability calculated as a mean from several independent experiments shown as mean ± SEM. Ca^{2+} dependences of tyrosine-phosphorylated IP_3R1 (WT-IP_3R1/Fyn Y528F, $n = 3$) and IP_3R1-Y353F (IP_3R1-Y353F/Fyn Y528F, $n = 7$) were fitted by the bell-shaped equation (*, $P < 0.05$ WT vs. Y353F by *t* test). (B) Representative traces of IP_3R1 activity at three different Ca^{2+} concentrations and the corresponding open probability (P_o), mean open time (t_o), and closed time (t_c) of the channels. Single channel openings are plotted as upward deflections; the open and closed (c) states of the channel are indicated by horizontal bars at the beginning of the traces.

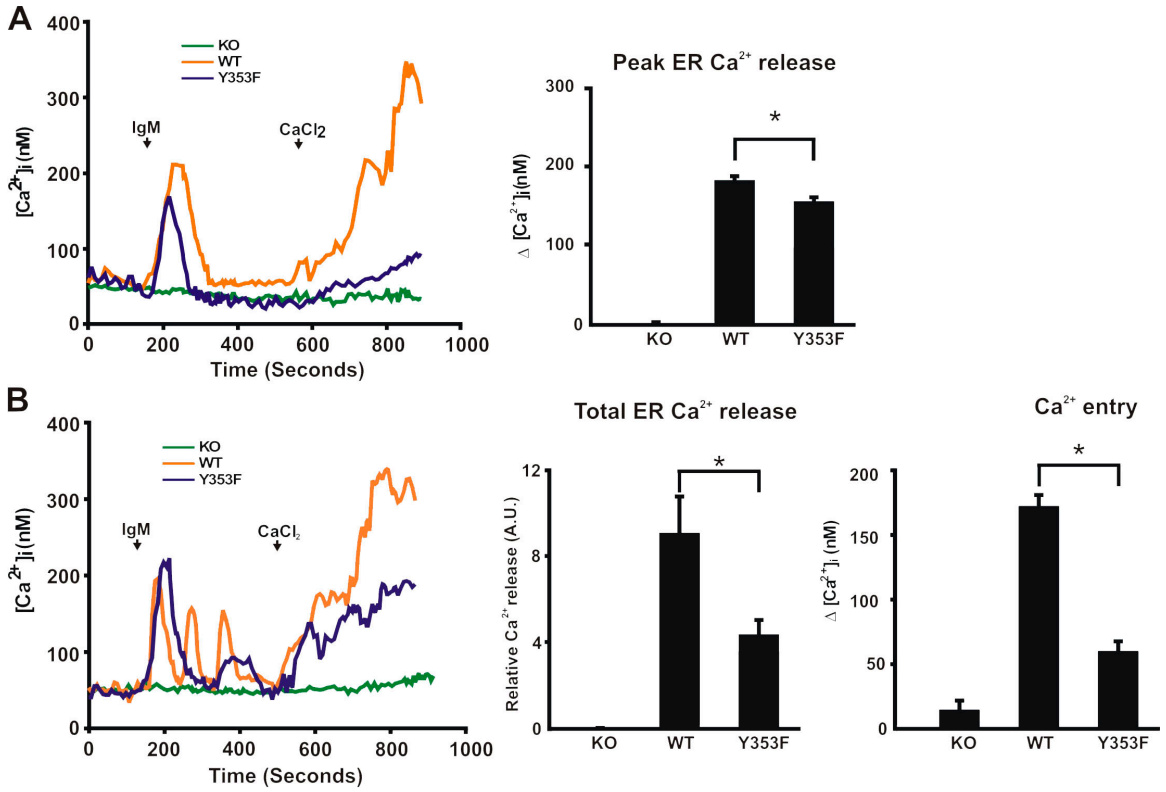

Figure 6. **Effects of IP_3R1-Y353F on Ca^{2+} influx after BCR stimulation.** (A) Peak of ER Ca^{2+} release measured in single cells upon BCR stimulation. Cytosolic Ca^{2+} was measured in a nominally Ca^{2+}-free medium. 5 μg/ml of anti-IgM antibody and 1 mM $CaCl_2$ were applied at time points indicated by arrows. The histogram shows the peak of Ca^{2+} release in WT-IP_3R1, IP_3R1-Y353F, and IP_3R-KO cells upon stimulation. Both oscillating and nonoscillating cells were used in the analyses and only the initial peak of Ca^{2+} release was measured in the stimulated cells. (B) Total ER Ca^{2+} release measured in single cells upon BCR stimulation. (left) Representative traces of Ca^{2+} oscillations observed in both WT-IP_3R1– and IP_3R1-Y353F–expressing cells upon IgM stimulation. (middle) The total $[Ca^{2+}]_i$ upon IgM stimulation with WT-IP_3R1–expressing cells showing approximately twofold increase relative to Ca^{2+} release in comparison to IP_3R1-Y353F–expressing cells (8.9 + 1.87 vs. 4.27 + 0.83; *, $P < 0.05$). (right) Quantification of total BCR-induced Ca^{2+} entry. The total Ca^{2+} entry of IP_3R-KO ($n = 54$), WT-IP_3R1–expressing ($n = 33$), and IP_3R1-Y353F–expressing cells ($n = 21$) is shown. Data represent the mean ± SEM (*, $P < 0.05$ WT vs. Y353F by *t* test). Total ER Ca^{2+} release and Ca^{2+} entry histograms were plotted by measuring the area under the curve after stimulation. All cells that responded to stimulation by IgM were analyzed.

IP_3R1-Y353 phosphorylation enhances Ca^{2+} entry in B lymphocytes

We previously showed that IP_3R1-Y353 phosphorylation slows the decay of the Ca^{2+} release transient upon B cell activation (Cui et al., 2004). To further examine both BCR-induced ER Ca^{2+} release and influx, single-cell studies were conducted using IP_3R null DT40 B cell lines (IP_3R-KO; Sugawara et al., 1997) stably transfected with either WT-IP_3R1 or IP_3R1-Y353F. Expression levels of WT-IP_3R1 and IP_3R1-Y353F in the stably transfected DT40 cell lines were comparable (unpublished data). IP_3R-KO cells exhibited no BCR-induced ER Ca^{2+} release and the addition of extracellular Ca^{2+} did not trigger Ca^{2+} influx (Fig. 6, A and B). Both WT-IP_3R1 and IP_3R1-Y353F cells responded to BCR stimulation manifested as IP_3-induced ER Ca^{2+} release (Fig. 6, A and B). Upon BCR stimulation, both the amplitude of the first peak of Ca^{2+} release and the total Ca^{2+} release were increased in DT40 cells expressing WT-IP_3R1 as compared with IP_3R1-Y353F–expressing cells (Fig. 6, A and B). Discrete Ca^{2+} oscillations, representing cyclical Ca^{2+} release from and reuptake into ER stores, were observed in ~30% of WT-IP_3R1–expressing cells, compared with <10% of IP_3R1-Y353F cells (Fig. 6 B), whereas only a single peak of ER Ca^{2+} release was observed in the remaining cells studied. This suggests that the phosphorylation of IP_3R1 at Y353 can increase the likelihood that the cell will oscillate upon lymphocyte activation. ER Ca^{2+} loading was similar and the pharmacological emptying of the ER using the SR/ER Ca^{2+} ATPase inhibitor thapsigargin showed that the Ca^{2+} entry machinery was otherwise intact in WT-IP_3R1– versus IP_3R1-Y353F–expressing cells (Fig. S1, available at http://www.jcb.org/cgi/content/full/jcb.200708200/DC1). Also, upon addition of extracellular $CaCl_2$, Ca^{2+} influx was significantly reduced in IP_3R1-Y353F–expressing cells compared with WT-IP_3R1–expressing cells in the time measured (Fig. 6 B), suggesting that in cells expressing IP_3R1-Y353F, the kinetics of Ca^{2+} influx are slower in comparison to WT-IP_3R1–expressing cells. Collectively, these data suggest that tyrosine phosphorylation of IP_3R1 at Y353 triggers greater emptying of ER Ca^{2+} stores, thereby causing greater Ca^{2+} influx via capacitative Ca^{2+} entry.

NFAT activity is enhanced by the phosphorylation of IP_3R1-Y353

Elevation of $[Ca^{2+}]_i$ triggers NFAT translocation to the nucleus, eventually leading to IL-2 production (Koretzky and Myung, 2001).

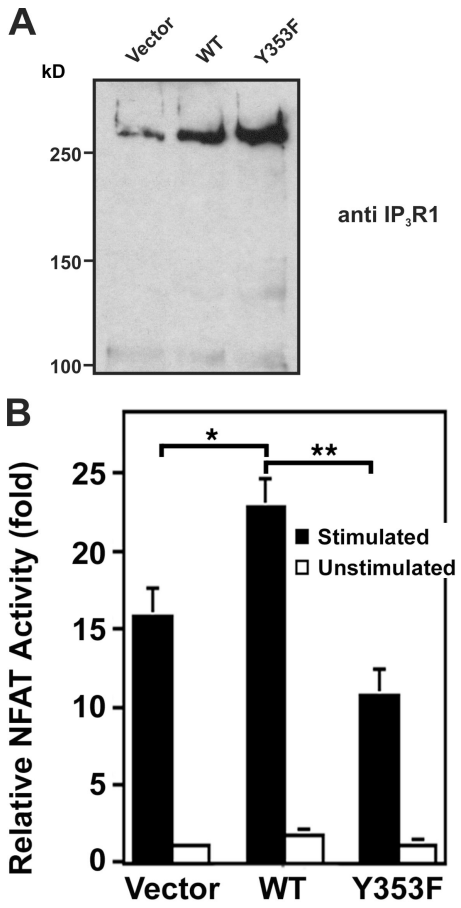

Figure 7. **Effect of IP_3R1 Y353 phosphorylation on NFAT activity.** (A) Immunoblotting of lysates from 10^6 transfected Jurkat T cells with anti-IP3R1 antibody showed comparable overexpression of WT-IP3R1 and IP3R1-Y353F. (B) Relative NFAT-dependent luciferase activity. 10^6 Jurkat cells were transiently transfected with WT-IP_3R1, IP_3R1-Y353F, or pcDNA3.1 vector together with an NFAT–firefly luciferase reporter assay construct and a TK-Renilla luciferase construct as a control for luciferase transfection efficiency. After stimulation with OKT3 (anti-CD3 antibody), cells were lysed and the lysates were assayed for NFAT-luciferase activity, quenched, and assayed for TK-luciferase activity in triplicate. NFAT activity is expressed as relative NFAT luminescence normalized to TK luminescence and adjusted for IP_3R1 expression levels. The results are shown as fold stimulation over nonstimulated vector control. Data were presented as the mean ± SEM of seven independent Jurkat preparations assayed in triplicate. (*, $P < 0.05$ WT vs. vector by *t* test; **, $P < 0.05$ WT vs. Y353F by *t* test).

Previous studies revealed that DT40 cells expressing only IP_3R1 exhibited decreased Ca^{2+} oscillations upon IgM stimulation (Miyakawa et al., 1999) and that decreasing the frequency of Ca^{2+} oscillations significantly mutes the NFAT response (Dolmetsch et al., 1998). Also, in lymphocytes, which express all three IP_3R isotypes, there appears to be considerable cooperativity in terms of the Ca^{2+} response upon lymphocyte stimulation (Miyakawa et al., 1999). Thus, to best address whether impaired Ca^{2+} influx observed in IP_3R1-Y353F–expressing cells affected downstream responses, Jurkat cells were transiently cotransfected with an NFAT–luciferase reporter construct and either an empty vector, WT-IP_3R1, or IP_3R1-Y353F. Immunoblotting of transfected cell lysates revealed the levels of WT-IP_3R1 and IP_3R1-Y353F (Fig. 7 A). In stimulated cells expressing WT-IP_3R1, NFAT activity (normalized to the level of IP_3R1 expression as shown in Fig. 7 A) was increased ~1.5-fold compared to vector-transfected cells (Fig. 7 B). This increase was significantly blunted in cells expressing IP_3R1-Y353F (Fig. 7 B). Collectively, these data suggest that phosphorylation of IP_3R1 at Y353 ensures robust NFAT activation.

Discussion

In this paper, we demonstrate that IP_3R1-Y353 phosphorylation is important for antigen-induced Ca^{2+} signaling during lymphocyte activation. $[Ca^{2+}]_i$ must be elevated for several hours after lymphocyte activation to ensure effective activation of downstream events such as IL-2 production (Huppa et al., 2003). The elevation of $[Ca^{2+}]_i$ is supported by ER Ca^{2+} store depletion, triggering sustained CRAC channel activation. Although recent work has revealed that the ER transmembrane protein STIM1 communicates ER store depletion to CRAC channels (Zhang et al., 2005), thereby triggering Ca^{2+} influx across the plasma membrane, mechanisms used by the cell to maintain depleted ER stores remain unclear. Although IP_3Rs constitute the primary ER Ca^{2+} release channel in lymphocytes, the role of IP_3Rs in mediating sustained ER depletion has been questioned. This is primarily because bulk $[IP_3]$ decreases to basal levels shortly after T cell activation (Guse et al., 1993; Sei et al., 1995) and $[Ca^{2+}]_i$ is elevated to levels that inhibit IP_3R1 channel activity in single-channel studies (Bezprozvanny et al., 1991).

In various cell types, physiological responses to extracellular agonists elicit sustained IP_3R activation. The formation of signaling complexes bringing IP_3Rs in close apposition to the cellular IP_3-generating machinery is believed to facilitate the activation of the channel even as global $[IP_3]$ decreases. In neurons, coclustering of bradykinin receptors with IP_3Rs creates a locally elevated IP_3 environment upon receptor stimulation (Delmas et al., 2002). Additionally, in kidney cells, IP_3R complexes with Na/K ATPase, Src, and PLC-γ1, creating sites of locally elevated IP_3 production (Yuan et al., 2005). We show that upon T cell activation, clustering of IP_3R1 phosphoY353 with the TCR and association of IP_3R1 with LAT can also create a locally elevated IP_3 environment, ensuring activation of IP_3Rs even as global IP_3 levels are decreasing. Moreover, modeling studies have shown that receptor clustering decreases the activation threshold and increases the response range to ligand (Bray et al., 1998). Collectively, with the phosphorylated receptor's increased affinity for IP_3 (Cui et al., 2004), the clustering of phosphorylated IP_3R1 upon T cell activation suggests a novel mechanistic solution to the problem of rapidly decreasing $[IP_3]$.

Recently, it has been shown that T cell activation is mediated and sustained by TCR signaling microclusters, which form on the cell surface (Yokosuka et al., 2005). Interestingly the stimulated T cell in Fig. 1 A reveals a colocalization pattern between the TCR and IP_3R1 phosphoY353, which is suggestive of signaling microclusters, specifically in the TCR–IP_3R1 phosphoY353 colocalization observed near the region where the antibody-mediated TCR clustering is the strongest. This is more clearly observed in the cell spreading assay in Fig. 2 B. It appears that both CD3 and IP_3R1 phosphoY353 are coclustered at the center and edges of the stimulated cell. The staining of both

proteins appears more punctuate in the periphery of the cell, with the clusters at the edge of the cell resembling signaling microclusters. The distribution of phosphorylated IP_3R1 into microclusters suggests the formation of discrete sites of ER–plasma membrane (PM) junctions, where maximal activation of phosphorylated IP_3R1 could occur, which is reminiscent of the ER–PM junctions observed upon thapsagargin-induced ER Ca^{2+} release in Jurkat T cells (Luik et al., 2006; Wu et al., 2006).

Additionally, because cytosolic Ca^{2+} levels must remain elevated for 2–10 h after T cell activation (Huppa et al., 2003), persistent phosphorylation of IP_3R1-Y353 even 60 min after the initial T cell activation event provides for sustained receptor activation, ensuring both discrete and controlled ER Ca^{2+} release even as global $[IP_3]$ decreases.

At the single channel level, phosphorylation of IP_3R1 at Y353 increases the channel's sensitivity to IP_3, allowing increased IP_3-dependent ER Ca^{2+} release at $[IP_3] < 10$ μM and reduces Ca^{2+}-dependent inactivation of IP_3R1 in the physiological range of $[Ca^{2+}]$ that occurs during lymphocyte activation, allowing for more efficient IP_3R1 activation at decreasing $[IP_3]$. It should be noted that the difference in Ca^{2+}-dependent activation of tyrosine-phosphorylated channels can be explained in part by the concurrent difference in IP_3 sensitivity. We found that at higher $[IP_3]$, the difference in Ca^{2+}-dependent activation between phosphorylated and nonphosphorylated channels was reduced. Thus, given the complex relationship between Ca^{2+}- and IP_3-dependent effects on IP_3R1 channel activity, it is likely that the responses observed in cells represent combined effects. We propose that phosphorylation of IP_3R1 at Y353 provides a mechanism for maintaining IP_3R1 channel activity in the presence of globally decreasing $[IP_3]$ and inhibitory cytosolic $[Ca^{2+}]$.

In single cell studies, WT-IP_3R1–expressing cells exhibited increased ER Ca^{2+} release and increased Ca^{2+} oscillations from the ER upon IgM stimulation in comparison to IP_3R1-Y353F–expressing cells. This increased ER Ca^{2+} release in WT-IP_3R1–expressing cells translated to increased Ca^{2+} influx across the plasma membrane. Current work detailing the communication between depleted ER stores and CRAC channels on the plasma membrane suggests that STIM1 is essential for communicating the level of ER Ca^{2+} to CRAC channels. Depletion of STIM1 has been shown to trigger decreased store-operated Ca^{2+} entry and a loss of CRAC channel activation (Liou et al., 2005; Roos et al., 2005). Recent work has shown that upon ER Ca^{2+} depletion, STIM1 reorganizes into discrete puncta at specific sites on the ER and colocalizes and potentially interacts with CRAC channels on the plasma membrane (Roos et al., 2005; Zhang et al., 2005; Luik et al., 2006; Wu et al., 2006; Yeromin et al., 2006). These closely apposed ER–PM junctions appear to be discrete sites of Ca^{2+} entry on the plasma membrane surface and imply a locally regulated elementary unit of store-operated Ca^{2+} entry. These recent findings strengthen the argument for the formation of spatially restricted ER–PM junctions on T cells, where signaling microdomains can occur and local regulation of Ca^{2+} signaling can be observed. It would be interesting to determine the localization of phosphorylated IP_3R1 relative to the STIM1-CRAC channel signaling unit upon T cell activation to determine if the phosphorylated receptor colocalizes with or modulates local Ca^{2+} signaling dynamics. Also, recent work has suggested that plasma membrane–localized IP_3R1s influence Ca^{2+} influx (Dellis et al., 2006). As such, the contribution of plasma membrane–localized, Y353-phosphorylated WT-IP_3R1 to the increased Ca^{2+} influx observed upon addition of extracellular Ca^{2+} is a possibility that cannot be excluded.

The downstream effect of increased ER Ca^{2+} release and influx is clearly demonstrated in the increased NFAT activity observed in Jurkat cells expressing WT-IP_3R1, a response that is blunted in IP_3R1-Y353F–expressing cells.

Thus, in a model of sustained receptor activation, as global $[IP_3]$ decreases and $[Ca^{2+}]$ reaches levels that inhibit nonphosphorylated IP_3R, IP_3R1 phosphoY353 is clustered on the ER in close proximity to the TCR, creating a spatially restricted signaling microdomain. Additionally, IP_3R1 phosphoY353 exhibits increased sensitivity to varying $[IP_3]$ and exhibits less channel inhibition at increasing $[Ca^{2+}]$, thereby allowing it to remain active at inhibitory $[Ca^{2+}]$. This sustained receptor activity contributes to elevating cytosolic Ca^{2+} levels both by ER Ca^{2+} release and CRAC channel activation, thereby ensuring robust lymphocyte proliferation (Fig. 8).

Materials and methods

Antibodies

Antibodies that recognize IP_3R1 and IP_3R1 phosphoY353 have been described previously (Cui et al., 2004). Antiphosphotyrosine 4G10 and mouse anti-LAT (Millipore); mouse anti–chicken IgM M4 (SouthernBiotech); mouse anti-CD3 OKT3 (Ortho Biotech); and anti–mouse IgG (Sigma-Aldrich) were used.

Cell culture and transfection

Jurkat T lymphocytes, ANJ3 LAT–deficient cells (provided by L. Samelson, National Institutes of Health, Bethesda, MD), and ZAP-70 null cells were cultured in RPMI 1640 medium containing 8% FBS, 100 U/ml penicillin, and 100 μg/ml streptomycin at 37°C in a humidified incubator (Thermo Fisher Scientific) with 5% CO_2. Chicken DT40 B cells and stable IP_3R1-transfected cell lines were cultured as described previously (Cui et al., 2004). HEK293 cells were maintained in DME supplemented with 10% FBS and transfected with plasmids using Lipofectamine 2000 according to the manufacturer's instructions (Invitrogen).

Single channel recording and data acquisition

Microsomes from HEK293 cells expressing WT-IP_3R1 cotransfected with Fyn Y528F, WT-IP3R1 cotransfected with Fyn K296M, or IP_3R1-Y353F cotransfected with Fyn Y528F were prepared as described previously (Kaznacheyeva et al., 1998). In brief, pellets were resuspended in homogenization buffer A (1 mM EDTA, 50 mM Tris-HCl, and 1 mM DTT, pH 8.0) supplemented with protease inhibitors and homogenized with a glass homogenizer (Teflon; DuPont). After a second homogenization step with buffer B (0.5 M sucrose, 1 mM EDTA, 20 mM Hepes, and 1 mM DTT, pH 7.5), the cell lysate was centrifuged at 1,000 *g* for 10 min. Consecutive supernatants were centrifuged at 10,000 *g* for 15 min and 100,000 *g* for 124 min (rotor AH-629; Ultra Pro 80; Sorvall). The pellet from the last centrifugation was resuspended in buffer C (10% sucrose and 10 mM MOPS, pH 7.0).

The recombinant IP_3R1s were reconstituted by spontaneous fusion of microsomes into the planar lipid bilayer (mixture of phosphatidylethanolamine and phosphatidylserine in a 3:1 ratio; Avanti Polar Lipids, Inc.). Planar lipid bilayers were formed across a 200-μm aperture in a polysulfonate cup (Warner Instruments), which separated two bathing solutions (1 mM EGTA, 1 mM HEDTA, 250/125 mM Hepes/Tris, 50 mM KCl, and 0.5 mM $CaCl_2$, pH 7.35, as a cis solution; and 53 mM $Ba[OH]_2$, 50 mM KCl, and 250 mM Hepes, pH 7.35, as a trans solution). After incorporation, IP_3R1 channels were activated with 2 μM IP_3 and the activity was recorded in the presence of 2 μM ruthenium red and 1 mM Na-ATP. Concentration of free Ca^{2+} in the cis chamber ranged from 80 nM to 2.5 μM by consecutive addition of $CaCl_2$ from 20-mM stock and was calculated with WinMaxC program (version 2.50; http://www.stanford.edu/~cpatton/maxc.html; Bers et al., 1994).

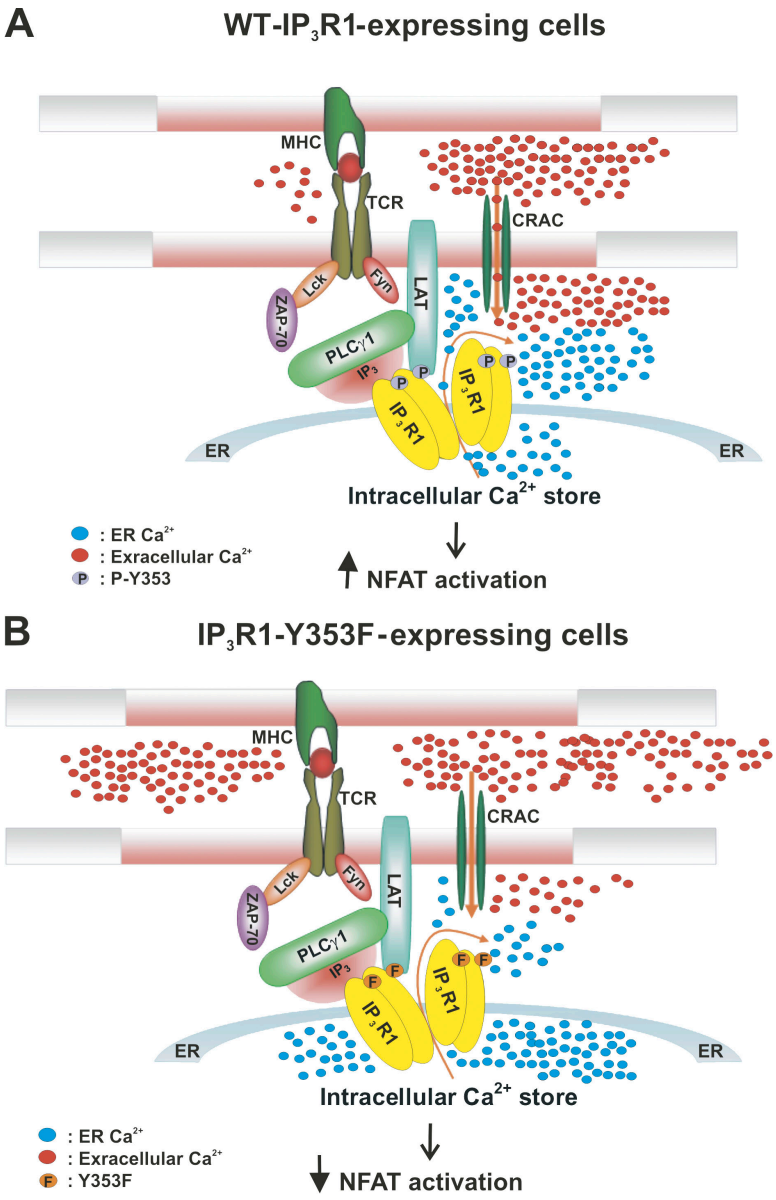

Figure 8. **Model of IP_3R1-TCR signal microdomain formation upon T cell activation.** (A) Activation of the TCR via interaction with an antigen-presenting cell causes recruitment and activation of Src family tyrosine kinases (Lck and Fyn). Antigen receptor engagement also induces capping of the TCR and phosphorylated IP_3R1 Y353 at the site of lymphocyte activation. Src family tyrosine kinases phosphorylate and activate ZAP-70. ZAP-70 phosphorylates the adaptor protein LAT and induces recruitment and activation of PLCγ-1 to LAT. LAT also associates with IP_3R1, bringing it closer to the signaling complex. IP_3R1 is phosphorylated at Y353 by Fyn and activated by local [IP_3], thereby triggering ER Ca^{2+} release, which couples to the activation of CRAC channels and induces Ca^{2+} influx and NFAT activation. (B) In lymphocytes expressing an IP_3R1-Y353F mutant receptor, loss of the phosphorylation site on IP_3R1 leads to decreased Ca^{2+} release from ER Ca^{2+} stores, which couples to decreased CRAC channel activation, causing decreased Ca^{2+} influx and leading to decreased NFAT activation.

In IP_3 dependence experiments, the activity of the channels was measured in the presence of 173 nM free Ca^{2+}, 2 μM ruthenium red, and 1 mM Na-ATP at an IP_3 concentration range of 10 nM to 50 μM. Single channel currents were recorded at 0 mV using the Axopatch 200A patch clamp amplifier (MDS Analytical Technologies) in gap-free mode, filtered at 500 Hz, and digitized at 4 kHz. Data acquisition was performed using Digidata 1322A and Axoscope 9 software (both from MDS Analytical Technologies). The recordings were stored on a computer (Pentium) and analyzed using pClamp 6.0.2 (MDS Analytical Technologies) and Origin software (6.0; OriginLab). The data in Ca^{2+}- and IP_3-dependence experiments was fitted with the curves as described previously (Tang et al., 2003). Only channels that exhibited maximum channel open probability exceeding 2% were included in the data analyses.

Cytosolic Ca^{2+} measurement

For single-cell calcium imaging, DT40 cells were loaded with 2 μM Fura-2/AM in culture medium at 37°C for 20 min, washed twice with culture medium, and washed once with nominally Ca^{2+}-free medium (107 mM NaCl, 7.2 mM KCl, 1.2 mM $MgCl_2$, 10 mM glucoses, and 20 mM Hepes, pH 7.2). Glass coverslips coated with poly-L-lysine were placed in a perfusion chamber (Photon Technology International) mounted on the stage of the microscope. Ca^{2+} images were captured as described previously (Cui et al., 2002). Only WT-IP_3R1– and IP_3R1-Y353F–expressing lymphocytes that showed Ca^{2+} release upon BCR stimulation were used for the data analysis. For the measurement of the peak of $[Ca^{2+}]_i$, cells that showed only a single peak of Ca^{2+} release and exhibited oscillations were included in the histogram analysis. For oscillating cells, only the first peak of Ca^{2+} release was measured. For total ER Ca^{2+} release measurements, all cells that showed Ca^{2+} release upon IgM addition were measured. The analysis included the multiple Ca^{2+} release events observed in oscillating WT-IP_3R1– and IP_3R1-Y353F–expressing cells. Additionally, total $[Ca^{2+}]_i$ release upon IgM stimulation was calculated by measuring the area (Fura2 ratio subtracted from baseline and integrated with time) for all cells showing release upon IgM stimulation.

Ca^{2+} entry was calculated by integrating the peak $[Ca^{2+}]_i$ with respect to time 5 min after the introduction of 1.5 mM $CaCl_2$. 1,500 s after addition of 1mM Ca^{2+}, ionomycin and EGTA were added to calculate maximum and minimum Ca^{2+}. For cells treated with thapsagargin, no significant difference in Ca^{2+} entry was observed for the WT-IP_3R1–expressing cells when compared with IP_3R1-Y353F–expressing cells upon addition of extracellular Ca^{2+}. All measurements shown are representative of three to five independent experiments.

NFAT luciferase assay

10^6 Jurkat cells were cotransfected with 3 μg WT-IP_3R1 or IP_3R1-Y353F plasmids with a 2-μg NFAT-luciferase plasmid and a 15-ng pRL–thymidine

kinase (TK) control plasmid using Lipofectamine 2000 in 24-well plates. 36 h after transfection, cells were split into two groups and were either stimulated using 1 μg/ml OKT3 anti-CD3 antibody or not stimulated as a control for 7 h, respectively. A luciferase assay was performed using a dual-luciferase assay (Promega) according to the manufacturer's instructions. The NFAT activity was expressed as fold excess over unstimulated cells for all three populations of cells (vector alone, WT-IP_3R1–transfected, and Y353F IP_3R1) and was normalized for IP_3R1 expression. Data are presented as the mean ± SEM of seven independent experiments each performed in triplicate. Statistical significance was determined using a *t* test.

Cell stimulation, immunoprecipitation, and immunoblotting

For the LAT coimmunoprecipitation experiment, 2×10^8 cells of each cell type were stimulated by incubating with 25 μg/ml anti-CD3 mAb (OKT3) at 37°C for 2 min followed by 15 μg/ml goat anti–mouse IgG for 5 min at 37°C. 10 ml of ice-cold PBS was added to stop stimulation and cells were harvested and lysed for immunoprecipitation and immunoblotting as described previously (Cui et al., 2004).

Confocal microscopy

For capping experiments imaging IP_3R1, Jurkat T cells were stimulated with 20 μg/ml OKT3 for 1 h on ice followed by cross-linking with 10 μg/ml of TRITC-labeled goat anti–mouse antibody (Jackson ImmunoResearch Laboratories) for 1 h on ice. Cells were pipetted onto poly-L-lysine–coated coverslips and incubated at 37°C for 5 min. The cells were then fixed with 3.7% formaldehyde for 10 min at room temperature. Cells were then washed, permeabilized, and stained with an antibody against IP_3R1 at 1:250 dilution or IP_3R1 phosphoY353 at 1:10,000 dilution followed by a secondary antibody stain of Alexa 488 goat anti–rabbit at 1:300 dilution (Invitrogen). For peptide blocking experiments, the IP_3R1 phosphoY353 antibody was preincubated with peptide at 4°C for 1 h before use. Coverslips were mounted on glass slides using Slowfade Gold antifade reagent (Invitrogen). The slides were examined with a laser scanning confocal microscope (LSM 510 META) with a 100× 1.3 Plan-Neofluor objective lens (both from Carl Zeiss, Inc.). All experiments were conducted at room temperature. Alexa 488 and TRITC were excited at 488 and 543 nm, respectively, and emissions were collected at 500–550 and >585 nm, respectively. Software (MetaView; Carl Zeiss, Inc.) was used for both acquisition and image processing. Z stack images were collected at an optical section thickness of 1 μM with maximum intensity projections of these sections computed to yield a projection image using MetaView software.

Cell spreading assay

The assay was performed as described previously (Bunnell et al., 2003) with minor modifications. Coverslips coated with anti-CD3 stimulatory antibody (clone HIT3a; BD Biosciences) were preincubated at 37°C for 30 min before use. Jurkat T cells were added, the cells were incubated at 37°C for various time points, and the stimulation was stopped by the addition of paraformaldehyde. The samples were fixed for 30 min at 37°C and permeabilized by the addition of 500 μg/ml digitonin (Sigma-Aldrich) for 5 min at room temperature. The samples were washed with PFN staining buffer (PBS, 10% FCS, and 0.02% azide) and blocked for 1 h with blocking buffer (2% goat serum and PFN buffer) at room temperature. The samples were then incubated with either anticalnexin at 1:1,000 (Sigma-Aldrich) or IP_3R1 phosphoY353 at 1:5,000 dilution, and 4G10 antiphosphotyrosine at 2 μg/ml dilution and anti-TCR (Santa Cruz Biotechnology, Inc.) at 2 μg/ml for 1 h at room temperature. The samples were incubated with secondary antibody stains of Alexa 488 goat anti–rabbit, Alexa 568 goat anti–mouse IgG1, and Alexa 680 goat anti–mouse IgG2b, all at 1:250 dilution (Invitrogen). The samples were washed and coverslips were mounted on glass slides using Slowfade Gold antifade reagent. The slides were examined at room temperature using a microscope (Axioimager.Z1) with a 63× 1.3 Plan-Neofluor objective lens and images were captured using a camera (Axiocam MRm; all from Carl Zeiss, Inc.). Axiovision 4.6.3 software (Carl Zeiss, Inc.) was used for both acquisition and image processing. Z stack images were collected at an optical section thickness of 0.5 μm through the entire cell using the Apotome slider on the Axioimager.Z1 with maximum intensity projections of these sections computed to yield a projection image for 3D surface rendering using Axiovision 4.6.3. Time-course analysis of Y353 phosphorylation was performed by comparing the fluorescence intensities of IP_3R1 phosphoY353 versus TCR for each cell slice in the z stack with the Metamorph imaging program. The area encompassing the clustered TCR was used to compare relative fluorescence intensities for each slice for each individual cell. Approximately 50 cells were analyzed for each time point from three independent experiments.

Statistical analysis

Statistical analysis was performed using the *t* test for paired samples. A computer program (Origin Pharmacology DoseResp; MicroCal) was used for statistical analysis. The EC_{50} values were calculated using SigmaPlot 8.0 (Systat Software Inc.) from a sigmoidal curve fitting of all the data points.

Online supplemental material

Fig. S1 shows that treatment of IP_3R-KO, WT-IP_3R1, or IP_3R1-Y353F DT40 cells with thapsigargin triggers comparable ER Ca^{2+} mobilization. Online supplemental material is available at http://www.jcb.org/cgi/content/full/jcb.200708200/DC1.

We thank Dr. Konstantina Alexandropoulos for assistance with NFAT measurements. We also thank Dr. Lawrence Samelson at the National Institutes of Health for the kind gift of the ANJ3 LAT-deficient cell line.

The authors declare that they have no conflicting financial interests.

Submitted: 29 August 2007
Accepted: 1 November 2007

References

Berridge, M.J., and R.F. Irvine. 1984. Inositol trisphosphate, a novel second messenger in cellular signal transduction. *Nature*. 312:315–321.

Bers, D.M., C.W. Patton, and R. Nuccitelli. 1994. A practical guide to the preparation of Ca2+ buffers. *Methods Cell Biol.* 40:3–29.

Bezprozvanny, I., J. Watras, and B. Ehrlich. 1991. Bell-shaped calcium response curves of Ins(1,4,5)P3- and calcium-gated channels from endoplasmic reticulum of cerebellum. *Nature*. 351:751–754.

Bray, D., M.D. Levin, and C.J. Morton-Firth. 1998. Receptor clustering as a cellular mechanism to control sensitivity. *Nature*. 393:85–88.

Bromley, S.K., W.R. Burack, K.G. Johnson, K. Somersalo, T.N. Sims, C. Sumen, M.M. Davis, A.S. Shaw, P.M. Allen, and M.L. Dustin. 2001. The immunological synapse. *Annu. Rev. Immunol.* 19:375–396.

Bunnell, S.C., V.A. Barr, C.L. Fuller, and L.E. Samelson. 2003. High-resolution multicolor imaging of dynamic signaling complexes in T cells stimulated by planar substrates. *Sci. STKE*. 2003:PL8.

Cui, J., J.S. Bian, A. Kagan, and T.V. McDonald. 2002. CaT1 contributes to the stores-operated calcium current in Jurkat T-lymphocytes. *J. Biol. Chem.* 277:47175–47183.

Cui, J., S.J. Matkovich, N. deSouza, S. Li, N. Rosemblit, and A.R. Marks. 2004. Regulation of the type 1 inositol 1,4,5-trisphosphate receptor by phosphorylation at tyrosine 353. *J. Biol. Chem.* 279:16311–16316.

Dellis, O., S.G. Dedos, S.C. Tovey, R. Taufiq Ur, S.J. Dubel, and C.W. Taylor. 2006. Ca2+ entry through plasma membrane IP3 receptors. *Science*. 313:229–233.

Delmas, P., and D.A. Brown. 2002. Junctional signaling microdomains: bridging the gap between the neuronal cell surface and Ca2+ stores. *Neuron*. 36:787–790.

Delmas, P., N. Wanaverbecq, F.C. Abogadie, M. Mistry, and D.A. Brown. 2002. Signaling microdomains define the specificity of receptor-mediated InsP(3) pathways in neurons. *Neuron*. 34:209–220.

Dolmetsch, R.E., K. Xu, and R.S. Lewis. 1998. Calcium oscillations increase the efficiency and specificity of gene expression. *Nature*. 392:933–936.

Douglass, A.D., and R.D. Vale. 2005. Single-molecule microscopy reveals plasma membrane microdomains created by protein-protein networks that exclude or trap signaling molecules in T cells. *Cell*. 121:937–950.

Espagnolle, N., D. Depoil, R. Zaru, C. Demeur, E. Champagne, M. Guiraud, and S. Valitutti. 2007. CD2 and TCR synergize for the activation of phospholipase Cgamma1/calcium pathway at the immunological synapse. *Int. Immunol.* 19:239–248.

Feske, S., Y. Gwack, M. Prakriya, S. Srikanth, S.H. Puppel, B. Tanasa, P.G. Hogan, R.S. Lewis, M. Daly, and A. Rao. 2006. A mutation in Orai1 causes immune deficiency by abrogating CRAC channel function. *Nature*. 441:179–185.

Guse, A.H., E. Roth, and F. Emmrich. 1993. Intracellular Ca2+ pools in Jurkat T-lymphocytes. *Biochem. J.* 291:447–451.

Huppa, J.B., M. Gleimer, C. Sumen, and M.M. Davis. 2003. Continuous T cell receptor signaling required for synapse maintenance and full effector potential. *Nat. Immunol.* 4:749–755.

Jayaraman, T., K. Ondrias, E. Ondriasova, and A.R. Marks. 1996. Regulation of the inositol 1,4,5-trisphosphate receptor by tyrosine phosphorylation. *Science*. 272:1492–1494.

Kaznacheyeva, E., V.D. Lupu, and I. Bezprozvanny. 1998. Single-channel properties of inositol (1,4,5)-trisphosphate receptor heterologously expressed in HEK-293 cells. *J. Gen. Physiol.* 111:847–856.

Khan, A.A., J.P. Steiner, M.G. Klein, M.F. Schneider, and S.H. Snyder. 1992. IP3 receptor: localization to plasma membrane of T cells and cocapping with the T cell receptor. *Science*. 257:815–818.

Khodakhah, K., and D. Ogden. 1993. Functional heterogeneity of calcium release by inositol trisphosphate in single Purkinje neurones, cultured cerebellar astrocytes, and peripheral tissues. *Proc. Natl. Acad. Sci. USA*. 90:4976–4980.

Koretzky, G.A., and P.S. Myung. 2001. Positive and negative regulation of T-cell activation by adaptor proteins. *Nat. Rev. Immunol.* 1:95–107.

Lewis, R.S. 2001. Calcium signaling mechanisms in T lymphocytes. *Annu. Rev. Immunol.* 19:497–521.

Liou, J., M.L. Kim, W.D. Heo, J.T. Jones, J.W. Myers, J.E. Ferrell Jr., and T. Meyer. 2005. STIM is a Ca2+ sensor essential for Ca2+-store-depletion-triggered Ca2+ influx. *Curr. Biol.* 15:1235–1241.

Luik, R.M., M.M. Wu, J. Buchanan, and R.S. Lewis. 2006. The elementary unit of store-operated Ca^{2+} entry: local activation of CRAC channels by STIM1 at ER–plasma membrane junctions. *J. Cell Biol.* 174:815–825.

Miyakawa, T., A. Maeda, T. Yamazawa, K. Hirose, T. Kurosaki, and M. Iino. 1999. Encoding of Ca2+ signals by differential expression of IP3 receptor subtypes. *EMBO J.* 18:1303–1308.

Monks, C.R., B.A. Freiberg, H. Kupfer, N. Sciaky, and A. Kupfer. 1998. Three-dimensional segregation of supramolecular activation clusters in T cells. *Nature*. 395:82–86.

Picard, L., J.F. Coquil, and J.P. Mauger. 1998. Multiple mechanisms of regulation of the inositol 1,4,5-trisphosphate receptor by calcium. *Cell Calcium*. 23:339–348.

Putney, J.W., Jr., L.M. Broad, F.J. Braun, J.P. Lievremont, and G.S. Bird. 2001. Mechanisms of capacitative calcium entry. *J. Cell Sci.* 114:2223–2229.

Roos, J., P.J. DiGregorio, A.V. Yeromin, K. Ohlsen, M. Lioudyno, S. Zhang, O. Safrina, J.A. Kozak, S.L. Wagner, M.D. Cahalan, et al. 2005. STIM1, an essential and conserved component of store-operated Ca^{2+} channel function. *J. Cell Biol.* 169:435–445.

Sei, Y., M. Takemura, F. Gusovsky, P. Skolnick, and A. Basile. 1995. Distinct mechanisms for Ca2+ entry induced by OKT3 and Ca2+ depletion in Jurkat T cells. *Exp. Cell Res.* 216:222–231.

Shibasaki, F., E.R. Price, D. Milan, and F. McKeon. 1996. Role of kinases and the phosphatase calcineurin in the nuclear shuttling of transcription factor NF-AT4. *Nature*. 382:370–373.

Sommers, C.L., C.S. Park, J. Lee, C. Feng, C.L. Fuller, A. Grinberg, J.A. Hildebrand, E. Lacana, R.K. Menon, E.W. Shores, et al. 2002. A LAT mutation that inhibits T cell development yet induces lymphoproliferation. *Science*. 296:2040–2043.

Sugawara, H., M. Kurosaki, M. Takata, and T. Kurosaki. 1997. Genetic evidence for involvement of type 1, type 2 and type 3 inositol 1,4,5-trisphosphate receptors in signal transduction through the B-cell antigen receptor. *EMBO J.* 16:3078–3088.

Svoboda, K., and Z.F. Mainen. 1999. Synaptic [Ca2+]: intracellular stores spill their guts. *Neuron*. 22:427–430.

Tang, T.S., H. Tu, Z. Wang, and I. Bezprozvanny. 2003. Modulation of type 1 inositol (1,4,5)-trisphosphate receptor function by protein kinase a and protein phosphatase 1alpha. *J. Neurosci.* 23:403–415.

Vig, M., C. Peinelt, A. Beck, D.L. Koomoa, D. Rabah, M. Koblan-Huberson, S. Kraft, H. Turner, A. Fleig, R. Penner, and J.P. Kinet. 2006. CRACM1 is a plasma membrane protein essential for store-operated Ca2+ entry. *Science*. 312:1220–1223.

Wu, M.M., J. Buchanan, R.M. Luik, and R.S. Lewis. 2006. Ca^{2+} store depletion causes STIM1 to accumulate in ER regions closely associated with the plasma membrane. *J. Cell Biol.* 174:803–813.

Yeromin, A.V., S.L. Zhang, W. Jiang, Y. Yu, O. Safrina, and M.D. Cahalan. 2006. Molecular identification of the CRAC channel by altered ion selectivity in a mutant of Orai. *Nature*. 443:226–229.

Yokosuka, T., K. Sakata-Sogawa, W. Kobayashi, M. Hiroshima, A. Hashimoto-Tane, M. Tokunaga, M.L. Dustin, and T. Saito. 2005. Newly generated T cell receptor microclusters initiate and sustain T cell activation by recruitment of Zap70 and SLP-76. *Nat. Immunol.* 6:1253–1262.

Yoneshima, H., A. Miyawaki, T. Michikawa, T. Furuichi, and K. Mikoshiba. 1997. Ca2+ differentially regulates the ligand-affinity states of type 1 and type 3 inositol 1,4,5-trisphosphate receptors. *Biochem. J.* 322:591–596.

Yuan, Z., T. Cai, J. Tian, A.V. Ivanov, D.R. Giovannucci, and Z. Xie. 2005. Na/K-ATPase tethers phospholipase C and IP3 receptor into a calcium-regulatory complex. *Mol. Biol. Cell*. 16:4034–4045.

Zhang, S.L., Y. Yu, J. Roos, J.A. Kozak, T.J. Deerinck, M.H. Ellisman, K.A. Stauderman, and M.D. Cahalan. 2005. STIM1 is a Ca2+ sensor that activates CRAC channels and migrates from the Ca2+ store to the plasma membrane. *Nature*. 437:902–905.